https://doi.org/10.5194/egusphere-2026-1748
Preprint. Discussion started: 2 April 2026

Aerosol Vertical Distributions Shaped by Boundary Layer Dynamics in a Coastal Urban Environment: Insights from the TRACER Campaign

Bo Chen[1,2], Seth A. Thompson[1], Brianna H. Matthews[1,3], Milind Sharma[1], Ron Li[1], Anita D. Rapp[1], Christopher J. Nowotarski[1], and Sarah D. Brooks[1]

[1]Department of Atmospheric Sciences, Texas A&M University, College Station, 77843, United States
[2]now at Colorado State University, Fort Collins, Colorado, 80521, United States
[3]now at Savannah River National Laboratory, Aiken, South Carolina, 29808, United States

Correspondence to: Sarah D. Brooks (sbrooks@tamu.edu)

Abstract. Aerosol vertical distributions are a major source of uncertainty in quantifying aerosol–cloud–climate interactions. Using observations collected during the 2022 TRACER campaign in Houston, Texas, we investigate how atmospheric boundary layer dynamics shape the vertical structure of aerosol populations in a coastal urban environment. Our lidar retrieval combines micropulse lidar backscatter with ground-based aerosol measurements to obtain aerosol concentration profiles. We introduce a new parameterized fitting function that captures the characteristic S-shaped aerosol profiles associated with boundary layer processes. This parameterization is applied to case studies demonstrating how boundary-layer dynamics, including turbulent mixing, capping inversion strength, and sea-breeze circulations, govern aerosol vertical distributions. Finally, we estimate aerosol vertical profiles from boundary layer height and gradients in potential temperature profile using our proposed aerosol profile parameterization function. These findings provide a physically grounded parameterization for inferring aerosol vertical profiles in locations where aerosol sampling is limited to surface measurements.

1 Introduction

Aerosols play a crucial role in influencing Earth's climate directly through interactions with solar radiation and indirectly through aerosol-cloud interactions (Haywood and Boucher, 2000; Kahn, 2012; Seinfeld et al., 2016). Aerosols scatter and absorb short and longwave radiation, thus contributing to direct aerosol radiative forcing (Szopa et al., 2023). Aerosols can also act as cloud condensation nuclei (CCN) and ice nucleating particles (INPs) to facilitate cloud formation, which leads to the aerosol indirect radiative effect (Twomey, 1977; Albrecht, 1989; Kanji et al., 2017; Burrows et al., 2022). In addition, light absorbing aerosols can heat the surrounding air, affect thermodynamic stability and cloud formation, and lead to the aerosol semi-direct radiative effect (Johnson et al., 2004). Therefore, to better quantify the radiative effects of aerosols, it is important to accurately characterize the spatial and temporal variations in aerosol concentration, size distributions, and physicochemical properties. Among these factors, aerosol vertical distributions significantly influence both the direct and

https://doi.org/10.5194/egusphere-2026-1748
Preprint. Discussion started: 2 April 2026

indirect radiative effects. In the presence of clouds, whether aerosols are located above or below the cloud substantially affects their direct radiative forcing (Choi and Chung, 2014). Under cloud-free conditions, the direct radiative effect of aerosols depends on the height of the aerosol layers (Mishra et al., 2015). Further, the magnitude of the aerosol direct radiative effect tends to increase with aerosol layer height in the ultraviolet and thermal infrared regions but decreases with aerosol layer height in the visible to near infrared range (Mishra et al., 2015). Simulations show that the altitude of aerosols critically influences how they are mixed in developing clouds, alter microphysical processes, and ultimately impact the strength of updrafts, cold pools, and resulting precipitation in deep convective systems (Lebo, 2014; Marinescu et al., 2017; Zhang et al., 2021). Long term observations demonstrate how different patterns of aerosol vertical distributions influence warm cloud properties, with aerosols suppressing cloud water production in continental environments but enhancing it in marine environments (Lin et al., 2023). Therefore, improving our understanding of the aerosol vertical distributions is one of the key challenges in reducing uncertainties in aerosol–cloud–climate interactions, refining climate models, and advancing our ability to predict future climate scenarios (Johnson et al., 2004; Kahn, 2012; Fan et al., 2016; Lin et al., 2023).

Both in situ and remote sensing observations have been used to examine aerosol vertical distributions, revealing complex spatial and temporal variability in aerosol characteristics. In situ aircraft measurements provide direct observations of aerosol concentration, size distribution, and chemical composition. Aircraft measurements show large concentrations of accumulation mode aerosols in the boundary layer, particularly in the northern extratropics due to anthropogenic emissions (Watson-Parris et al., 2019). Above the boundary layer top, new particle formation leads to a shift toward smaller particle sizes with increasing altitude (Watson-Parris et al., 2019). In clean marine regions, aerosol concentration can increase with altitude due to the homogeneous nucleation of small volatile particles at higher altitudes, while sea salt aerosols dominate at lower altitudes (Clarke and Kapustin, 2010). In more polluted marine regions, long range transport contributes to increased aerosol concentration above 4 km (Clarke and Kapustin, 2010). Over continental regions, emissions from urban and industrial sources result in large aerosol concentrations near the surface (Clarke and Kapustin, 2010). Analysis of aircraft measurements reveals that the thermodynamic stability of the atmospheric boundary layer has a significant influence on the shape of the aerosol vertical profile. When stable layers, such as nocturnal or frontal inversions, are present, vertical mixing is suppressed, trapping aerosols within the boundary layer and creating a sharp concentration gradient above it (Zhang et al., 2009).

Modeling studies also provide some insight on the factors that may control aerosol vertical distributions (Freire et al., 2016; Nissanka et al., 2018; Xiao and Taylor, 2002). The atmospheric boundary layer dynamics and processes also play a central role in shaping aerosol vertical profiles. The distribution of aerosols within the boundary layer is controlled by the balance between vertical turbulent transport and gravitational settling. When these processes are in equilibrium, the surface layer aerosol concentrations generally follow a power law relationship (Hoppel et al., 2002; Xiao and Taylor, 2002). Larger particles experience stronger gravitational settling, leading to a steeper concentration decline with height, while smaller

https://doi.org/10.5194/egusphere-2026-1748
Preprint. Discussion started: 2 April 2026

particles are more influenced by turbulent mixing, resulting in a more gradual decrease and a more uniform vertical distribution. Under unstable conditions, strong turbulent mixing distributes aerosols more evenly throughout the boundary layer, while in stable conditions, weak turbulence keeps aerosols concentrated near the surface (Freire et al., 2016; Nissanka et al., 2018). Since boundary layer mixing influences the vertical distributions of surface emitted aerosols like sea salt and mineral dust (Kipling et al., 2016), boundary layer evolution throughout the day may lead to corresponding diurnal changes in aerosol profiles (Zhang et al., 2023; Haman et al., 2012).

Despite the level of vertical detail they provide, aircraft in situ observations are limited in temporal and spatial coverage. Surface measurements can offer routine and continuous observations but cannot capture vertical information. Lidar measurements allow routine aerosol vertical profile measurement, yet optical measurements are strongly affected by aerosol hygroscopic growth. More comprehensive analysis method integrating both in situ observations and remote sensing techniques are needed to improve our understanding of the factors governing aerosol vertical distributions. This knowledge can be further used to predict aerosol vertical profiles when airborne and lidar measurements are not available and to provide more realistic aerosol data for aerosol-cloud interaction studies. During the 2022 TRacking Aerosol Convection interactions ExpeRiment (TRACER) field campaign, a suite of comprehensive atmospheric data, including thermodynamic profiles, ground-based lidar observations, and surface aerosol measurements, was collected across multiple sites in the Greater Houston, Texas area (Rapp et al., 2024; Jensen et al., 2025). Using our newly developed method by combining ground-based aerosol and lidar measurements, we retrieve aerosol vertical profiles informed by micropulse lidar backscatter coefficient corrected for relative humidity dependent hygroscopic growth, combined with surface measurements of aerosol, CCN, and INPs (Chen et al., 2025).

In this study, we combine aerosol profiles derived from lidar with meteorological observations to characterize typical aerosol vertical distributions in a coastal urban environment and to quantify how boundary layer height (BLH) and stability together control the shape of these profiles. We also provide a set of fitting functions that streamline aerosol vertical profile parameterization, facilitate the incorporation of aerosol vertical profiles into cloud-resolving models, and provide insights into understanding the physical processes governing aerosol vertical distributions. A further goal is to assess the extent to which aerosol vertical profiles can be predicted using only routine meteorological observations and surface aerosol measurements, in the absence of lidar observations.

https://doi.org/10.5194/egusphere-2026-1748
Preprint. Discussion started: 2 April 2026

2 Method

2.1 Field campaign and data collection

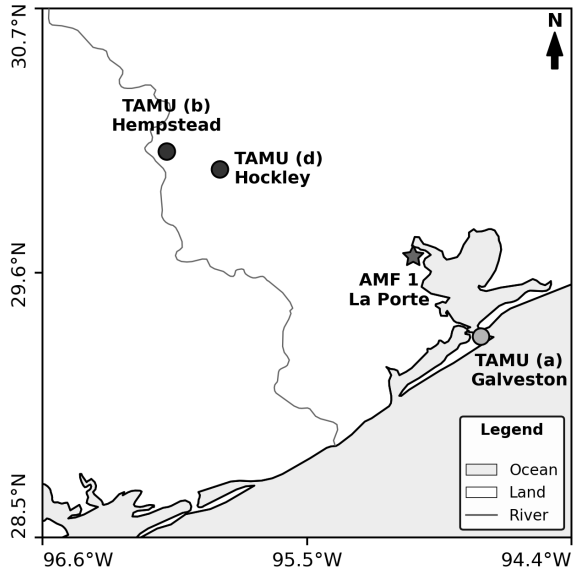

Figure 1 TRACER campaign sampling locations in the Houston, Texas, metropolitan area. The Texas A&M University sampling sites are marked with circles, the ARM AMF1 site is marked with a star. The map is reproduced from Figure 1 of Chen et al. (2025).

Our analysis focuses on data from the TRACER campaign, organized by the U.S. Department of Energy, from October 2021 through September 2022. The primary measurements were made in the Greater Houston Area, Texas. Throughout the campaign, the ARM Mobile Facility (AMF-1) operated continuously at La Porte, Texas shown in Figure 1 (Jensen et al., 2025). Additional aerosol and meteorological data were collected by deploying Texas A&M University's Rapid Onsite Atmospheric Measurement Van (ROAM-V) alongside radiosonde launches at multiple locations spanning coastal and inland environments (Figure 1) on selected days when isolated convection was expected (Rapp et al., 2024; Thompson et al., 2025a; Thompson et al., 2025b; Lei et al., 2025). As shown in Figure 1, the coastal site is in Galveston, Texas, while the inland sites include locations in Hempstead and Hockley, Texas.

https://doi.org/10.5194/egusphere-2026-1748
Preprint. Discussion started: 2 April 2026

2.2 Aerosol vertical profile retrieval using the micropulse lidar

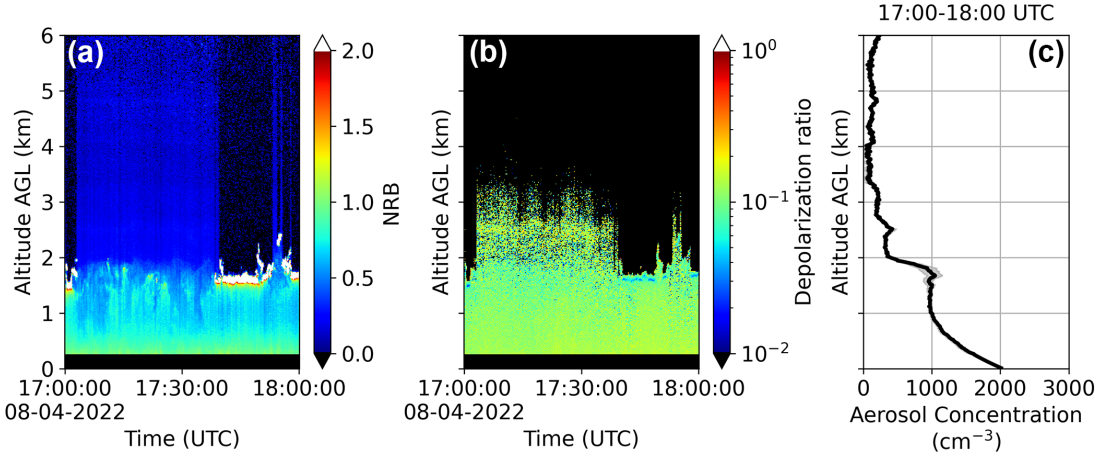

Figure 2 Micropulse lidar measurements on 4 August 2022, at AMF-1 site (a) normalized relative backscatter time-height plot (b) linear depolarization ratio time-height plot (c) retrieved aerosol concentration vertical profile.

In this work, we employ a method to integrate micropulse lidar and ground-based aerosol measurements to retrieve aerosol vertical distributions corrected for aerosol hygroscopic growth (Chen et al., 2025). Interested readers are referred to Chen et al. (2025) for methodological details. In brief, the procedure first applies an inversion to lidar measurements of attenuated backscatter to obtain an hourly time-averaged cloud-free aerosol backscatter coefficient profile. Next, we use the aerosol hygroscopicity parameter κ, along with Mie scattering theory, to account for aerosol hygroscopic growth at increased humidity measured by the radiosonde, allowing us to convert the retrieved ambient backscatter coefficient to its dry equivalent. The aerosol hygroscopicity parameter κ was estimated from Aerosol Chemical Speciation Monitor (ACSM) aerosol composition measurements collected during the TRACER campaign, with κ values provided by M. A. Zawadowicz (personal communication, 2025). This step is crucial because lidar measures optical signals affected by aerosol hygroscopic growth. As aerosols take up water, they grow in size, scatter more light, and increase the lidar backscatter signal without increasing aerosol concentration. Correcting for the aerosol hygroscopic growth effect prevents overestimation of aerosol concentration at altitudes with higher relative humidity. Finally, we scale the surface aerosol concentration measured by the condensation particle counter by the ratio of the dry backscatter at each level to that of the surface. Figure 2 shows a typical micropulse lidar measurement and aerosol profile retrieval result at the AMF1 site on 4 August 2022 from 17:00 to 18:00 UTC. The retrieved aerosol profile (Figure 2c) exhibits an approximately exponential decrease from the surface through the lowest 1 km, then remains relatively uniform up to ~2 km before sharply transitioning to a clean background concentration aloft.

https://doi.org/10.5194/egusphere-2026-1748
Preprint. Discussion started: 2 April 2026

2.3 Aerosol vertical profile fitting function

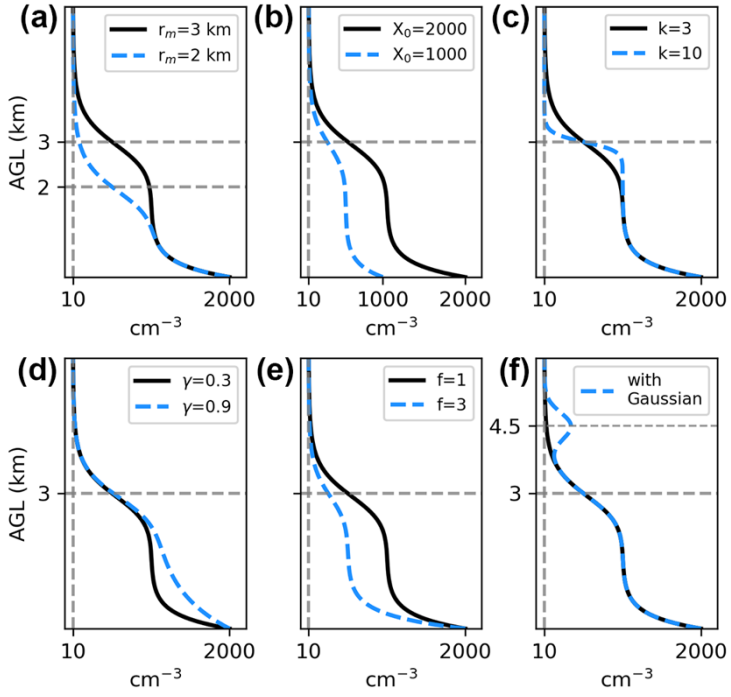

Figure 3 Effects of individual fitting function parameters on the aerosol vertical profile shape. Each panel varies one parameter while others are held constant. Solid black lines show the reference profile, and dashed blue lines show the parameter modified profiles. Horizontal gray dashed lines mark transition zone height r_m. Vertical gray dashed lines denote a constant concentration of 10 cm^{-3} (a) r_m shifts the height of the transition zone; (b) X_0 sets the surface concentration; (c) changing parameter k changes the sharpness of the transition; (d) changing parameter γ changes the shape of near surface decline in concentration; (e) changing parameter f influences the magnitude of the exponential decay; and (f) adds a Gaussian peak to represent an elevated aerosol layer.

https://doi.org/10.5194/egusphere-2026-1748
Preprint. Discussion started: 2 April 2026

From the retrieved aerosol profiles, we typically observe high near-surface concentrations, with a steep decrease immediately above the surface, a more gradual decline aloft, and then a sharp transition to low background concentrations in the free troposphere. To capture this behavior, we developed a fitting function (Equation 1) to parameterize the aerosol vertical profile data when no long range transported aerosol is present at upper altitudes, and aerosols primarily originate from near surface sources.

$$X(r) = \frac{X_0 - X_f}{1+f} \cdot \frac{1 + f e^{-\frac{r}{\gamma}}}{1 + \left(\frac{r}{r_m}\right)^{r_m k}} + X_f \quad (1)$$

where:

- r: vertical range from the lidar (km)
- $X(r)$: aerosol concentration at range r (cm^{-3})
- X_0: aerosol concentration at the surface (cm^{-3})
- X_f: aerosol concentration at the top of the vertical profile (cm^{-3})
- r_m: transition zone height above ground (km)
- k: sharpness of the transition zone (unitless)
- γ: near surface decay rate (unitless)
- f: exponential decay scaling factor (unitless)

Equation 1 is well suited for representing aerosol vertical profiles, as it combines an exponential decay function with a sigmoid function to describe the monotonic decrease with an S-shaped transition typically seen in the shape of retrieved aerosol profiles. As demonstrated in Figure 3, this function also anchors the concentration to aerosol concentration directly measurable at the surface, and allows flexible control of the profile shape. To arrive at this equation, we first defined the *transition zone* as the altitude range where aerosol concentration declines sharply from well-mixed lower tropospheric layer to free tropospheric background. The *transition zone height* r_m (measured from ground level) is defined as the midpoint of the transition zone. The value of r_m can be determined by fitting the Equation 1 to measured aerosol vertical distributions. While r_m may align with the top of the planetary boundary layer, that is not always true. To avoid confusion, we treat r_m strictly as the transition zone height, representing the altitude that characterizes the boundary between the low level aerosol layer and the cleaner air aloft. As shown in Figure 3a, adjusting r_m shifts the height of the transition zone without altering the surface aerosol concentration or the gradient at r_m. X_0 controls the aerosol concentration at the surface. Figure 3b demonstrates that modifying X_0 only affects the surface concentration without altering the relative shape of the vertical profile. X_f determines the aerosol concentration at the top of the vertical profile and X_f is set to 10 cm^{-3} in Figure 3. k determines how rapidly the aerosol concentration changes in the transition zone. As illustrated in Figure 3c, increasing k enhances the relative sharpness of the transition zone, causing a more abrupt decrease in aerosol concentration with height. γ and f affect how aerosol concentration decreases with height below the transition zone. The parameter γ, the near surface decay rate, controls the shape of the lowest portion of the profile by modifying the curvature of the exponential decay. Figure

https://doi.org/10.5194/egusphere-2026-1748
Preprint. Discussion started: 2 April 2026

170 3d shows that increasing γ changes the shape of near surface decline, affecting the lower portion of the profile. In this study, γ is chosen as 0.3 because this value consistently provided reliable fits across a wide range of profiles. Fixing γ to a set value also makes the fit more stable. When both γ and f are allowed to vary, they can compensate for each other, so many pairs of γ and f result in similarly good fits. Fixing γ reduces this trade-off and better constrains f and other parameters, resulting in a more robust and interpretable fit. According to Equation 1 and as shown in Figure 3e, the parameter f, the scaling factor,
175 scales the exponential decay term, thereby influencing the extent to which aerosol concentration decreases from the surface to the transition zone.

While Equation 1 models the monotonic, surface-anchored profiles typical of cases dominated by local emissions, it cannot represent distinct elevated aerosol layers that are separated from the boundary layer, such as those produced by long-range
180 transport or secondary particle formation aloft. In this study, the parameters of Equation 1 are constrained by near-surface aerosol measurements together with lidar-derived aerosol profiles. To represent elevated layers observed in the lidar profiles, one or more Gaussian peak terms can be added to Equation 1. Each Gaussian is centered at the altitude of an observed elevated layer and providing a simple parametric description of that feature. To avoid overfitting, we use as few Gaussian terms as necessary. Specifically, we allow at most two Gaussian terms when elevated layers are apparent. The fitting
185 function with N elevated aerosol layers is given by:

$$X_{\mathrm{aug}}(r) = \frac{X_0 - X_f}{1+f} \cdot \frac{1 + f e^{-\frac{r}{\gamma}}}{1 + \left(\frac{r}{r_m}\right)^{r_m k}} + \sum_{j=1}^{N} A_j \exp\left(-\frac{1}{2}\left(\frac{r - r_{c,j}}{\sigma_j}\right)^2\right) + X_f \quad (2)$$

Equation 2 adds N Gaussian terms to Equation 1, each representing an elevated aerosol layer centered at altitude $r_{c,j}$ with amplitude A_j and width σ_j. An example profile derived from Equation (2) with a single Gaussian term is illustrated in Figure 3f.

190 Given the boundary layer's influence on aerosol vertical profiles, BLH may be a critical factor determining profile shape, thus may be correlated with independent parameters in Equation 1. To facilitate our comparison of aerosol profiles to the BLH, we used two different BLH product developed in Lamer et al. (2024). The first is based on the bulk Richardson number (R_{ib}), which quantifies the relative effects of buoyancy and wind shear on turbulent mixing (Stull, 2012). A bulk Richardson number equal to 0.5 is used as the threshold to determine the top of the atmospheric boundary layer (Lamer et
195 al., 2024). The other approach is based on a thermodynamic method that separates the atmosphere into three stability regimes, using distinct potential temperature profile characteristics to identify the BLH in each case (Lamer et al., 2024; Liu and Liang, 2010). In this paper, the bulk Richardson number-based boundary layer height will be referred to as BLH-RiB, and the thermodynamic-based boundary layer height will be referred to as BLH-LL.

https://doi.org/10.5194/egusphere-2026-1748
Preprint. Discussion started: 2 April 2026

3 Results

In the following sections, we present three case studies from the TRACER campaign to illustrate how boundary layer processes, driven by diverse meteorological conditions, affect aerosol vertical distributions, and explain the mechanisms behind their observed variability. The aerosol profiles and their variability are further quantified by fitting Equations 1 and 2 to the data.

3.1 Case study: Aerosol stratification below a strong capping inversion

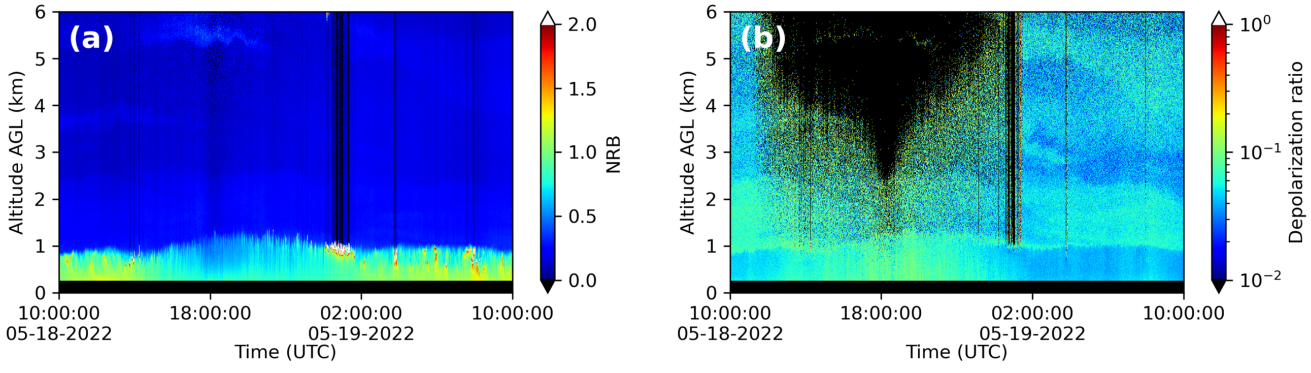

Figure 4 Micropulse lidar measurement from 10:00 UTC on 18 May to 10:00 UTC on 19 May 2022, at AMF-1 site (a) normalized relative backscatter time series. and (b) linear depolarization ratio time series with signal to noise ratio > 3.

The first case on 18–19 May 2022 showcases the evolution of the aerosol vertical profile within a well-mixed boundary layer capped by a strong temperature inversion. The largest normalized relative backscatter (NRB) is found close to the surface, forming a distinct boundary where it transitions to lower NRB around 1 km, above which elevated aerosol layers between 3 and 6 km are also visible (Figure 4a). Figure 4b more clearly reveals elevated aerosol layers through the depolarization ratio. The aerosol layer below 1 km exhibits a smaller NRB and larger depolarization ratio during the daytime, which mirrors the evolution of surface relative humidity, as shown in Figure S.1 (see appendix), where the relative humidity decreases from 100% at nighttime to 50% in the early afternoon. The larger relative backscatter and smaller depolarization ratios observed near the surface at night are due to greater humidity, causing aerosols to take up water and become larger and more spherical. In Figure 4b, one elevated aerosol layer can be identified between 1 km and 2.5 km, separated from the aerosol layer below 1 km. Relative humidity drops sharply around 1 km (Figure 5), and aerosol aloft are therefore more likely dry and less spherical, which increases the depolarization ratio. HYSPLIT back trajectories (Figure S.4) indicate that the low-level and 1–2.5 km layers being transported from over the Gulf of Mexico during the preceding 12–24 h. The pronounced relative humidity dependence of the depolarization ratio in these layers, together with the HYSPLIT results, suggest a major contribution from hygroscopic sea salt aerosol. Elevated aerosol layers between 3 and 6.6 km show large depolarization ratios, with the 5 km layer traced by 24-h HYSPLIT back trajectories to long range free tropospheric transport.

https://doi.org/10.5194/egusphere-2026-1748
Preprint. Discussion started: 2 April 2026

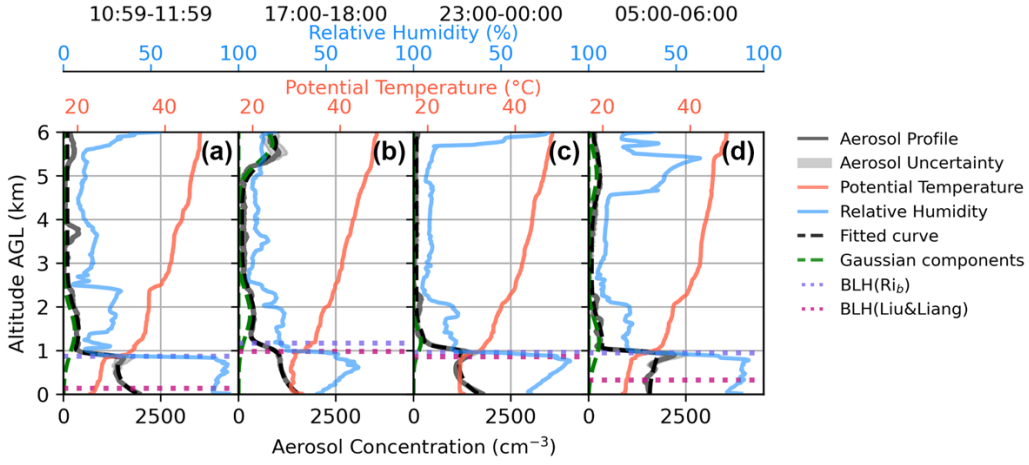

Figure 5 Retrieved vertical profiles of aerosol number concentration (gray solid lines), potential temperature profiles (solid red lines), relative humidity profile (solid blue lines), and curve fit aerosol vertical profile (dashed black lines) at the AMF-1 site on 18–19 May 2022. Green dashed lines indicate Gaussian components added to represent elevated aerosol layers. BLHs determined by the bulk Richardson number and the Liu & Liang method are shown as purple and magenta dotted horizontal lines, respectively. The curve fit profile closely overlaps the measured number-concentration profiles, so the gray lines can be difficult to distinguish from the black dashed lines where agreement is good. Each panel corresponds to a one-hour averaging window in UTC time: (a) 10:59–11:59 on 18 May, panel (b) 17:00–18:00 on 18 May, (c) 23:00–00:00 across 18–19 May, and (d) 05:00–06:00 on 19 May.

Aerosol, potential temperature, and RH profiles, as well as BLH estimates at different times of the day on 18–19 May 2022 are shown in Figure 5. The four aerosol profiles throughout the day are similar. For all four profiles, aerosol concentrations are approximately 1500 to 2000 cm^{-3} near the surface and decrease sharply to less than 500 cm^{-3} above 1 km altitude. Equation 2 is used to fit to the aerosol vertical profiles (with fit parameters listed in Table S.1). All four potential temperature profiles in Figure 5 show a strong inversion near 1 km, and BLH-RiB remains near this level throughout the day, closely matching the fitted transition zone height r_m. The co-variation between the aerosol profile and the potential temperature profile likely reflects a common boundary-layer evolution. The thermal structure could also limit vertical mixing and help shape the observed aerosol layering. Aerosol radiative effects may, in turn, reduce solar radiation at the surface and therefore surface heating, strengthening the inversion and helping to maintain the layering. The RH profile also exhibits features that align with the aerosol distributions. Below 1 km, RH reaches around 90% or higher except in the early afternoon (68.6% at 17:00–18:00 UTC), and it drops sharply near 1 km at the primary aerosol-layer top. This pattern is consistent with boundary-layer turbulent transport shaping both moisture and aerosol distributions. Note that the influence of RH and hygroscopic growth on the aerosol lidar signal has already been accounted for in the retrieval of the aerosol vertical profile (Chen et al., 2025).

BLH-LL, is 140 m in the early morning (10:59–11:59 UTC) and 320 m around midnight (05:00–06:00 UTC). BLH-RiB and BLH-LL are in general agreement in the early afternoon (17:00–18:00 UTC) and early evening (23:00–00:00 UTC). The BLH-LL accurately captures the diurnal cycle of boundary layer thermodynamics, correctly finding the shallow stable

https://doi.org/10.5194/egusphere-2026-1748
Preprint. Discussion started: 2 April 2026

boundary layer that develops near the surface during nighttime. Aerosols that accumulate within the deeper daytime boundary layer often remain suspended above the much shallower nocturnal layer, forming a residual layer at night.

The aerosol vertical profile in this case study is strongly governed by boundary layer processes, with well-mixed near surface layers during the day and residual layering at night. The aerosol profile exhibits sharp stratification near inversion layers, and elevated aerosol layers persist aloft, decoupled from surface influences. The vertical distributions thus highlight the importance of diurnal boundary layer evolution in shaping aerosol structure.

3.2 Case study: Aerosol profile under boundary layer development and collapse

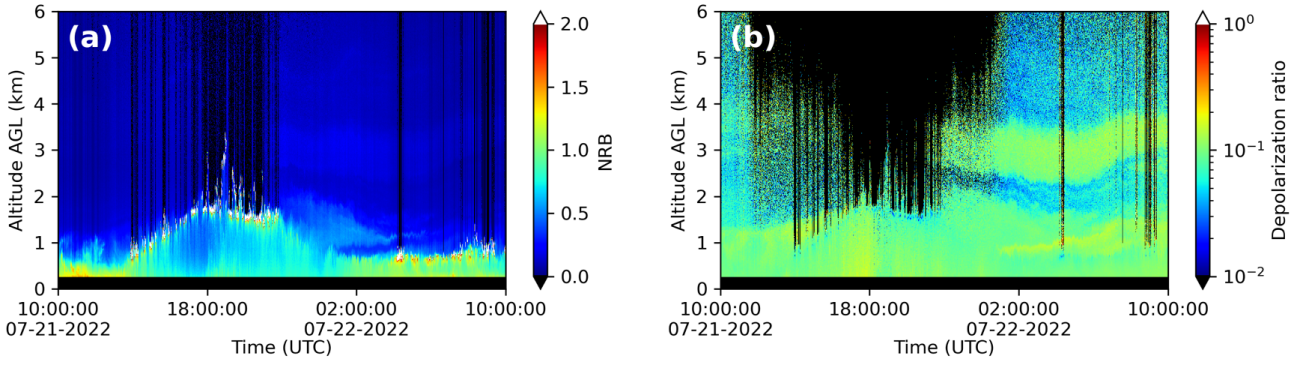

Figure 6 Micropulse lidar measurement from 10:00 UTC on 21 July to 10:00 UTC on 22 July 2022, at AMF-1 site (a) NRB time series (b) linear depolarization time series with signal to noise ratio > 3.

The second case, recorded on 21-22 July 2022, demonstrates the evolution of the aerosol vertical structure during the development and collapse of the daytime boundary layer. Figure 6 shows the 24-hour NRB and depolarization ratio measurements from the micropulse lidar, capturing the vertical structure of aerosols and clouds throughout the diurnal cycle. As seen in Figure 6a, shallow cumulus clouds developed during the local morning and extended to just below 2 km by local noon, marking the growth of the daytime boundary layer, whose top is often associated with boundary layer cumulus cloud top (Stull, 2012). By late afternoon, around 22:00 UTC, banded and optically thick cirrus moved over the site (shown in Figure S.5 in the Supplement). This coincided with reduced vertical mixing and an early collapse of the mixed layer, as indicated by a decrease in BLH from Figure 7b to Figure 7c. An elevated aerosol layer between approximately 2 and 4 km is visible in Figure 6b, which shows larger depolarization ratios in the 0–2 km and 2–4 km ranges, separated by a layer of smaller depolarization ratio in between. The elevated aerosol layer becomes more distinct in the evening hours and persists into the night. A similar elevated layer between around 2 and 4 km is also faintly visible in the backscatter signal of Figure 6a. The separation between the low-level aerosol layer and the elevated layer indicate possible stratification and limited vertical mixing

https://doi.org/10.5194/egusphere-2026-1748
Preprint. Discussion started: 2 April 2026

between these layers during the observation period. HYSPLIT back trajectories (Fig. S.4 in the Supplement) show the ~3 km layer arrived from the east along the Gulf Coast, unlike the low-level air mass, indicating the elevated layer is decoupled from the boundary layer and likely has a distinct source, potentially from long-range transport.

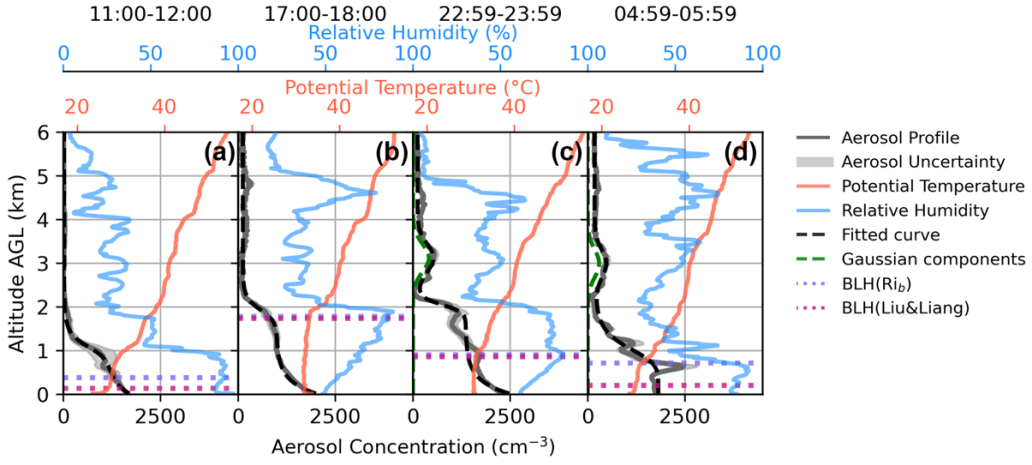

Figure 7 Measured vertical profiles of aerosol number concentration (gray solid lines), potential temperature profiles (solid red lines), relative humidity profile (solid blue lines), and curve fitted aerosol vertical profile (dashed black lines) at the AMF-1 site on 21–22 July 2022. Green dashed lines indicate Gaussian components added to represent elevated aerosol layers. Boundary layer heights determined by the bulk Richardson number and the Liu & Liang method are shown as purple and magenta dotted horizontal lines, respectively. The curve fit profile closely overlaps the measured number-concentration profiles, so the gray lines can be difficult to distinguish from the black dashed lines where agreement is good. Each panel corresponds to a one-hour averaging window in UTC time: (a) 11:00–12:00 on 21 July, panel (b) 17:00–18:00 on 21 July, (c) 22:59–23:59 on 21 July, and (d) 4:59–05:59 on 22 July.

Figure 7 presents aerosol vertical profiles, potential temperature, relative humidity, and BLHs at four different times. Surface aerosol concentrations remain consistently large throughout the 24-hour period, ranging approximately from 1700 to 2500 cm^{-3}. Equations 1 and 2 are used to curve fit the aerosol vertical profiles, as illustrated in dashed black lines in Figure 7. The profiles follow an S-shaped decrease in concentration, with the transition zone height r_m diagnosed from the fitted curve. One dominant aerosol layer is observed in early morning (11:00–12:00 UTC) and early afternoon (17:00–18:00 UTC) shown in Figure 7a-b. In the early morning, r_m is near 1 km, indicating the nighttime residual aerosol layer. By early afternoon, r_m rises to just below 2 km as the mixed layer deepens, as indicated by BLH-RiB and BLH-LL, which closely agree and coincide with r_m. The potential temperature structure is consistent with this evolution. In Figure 7a, a modest temperature inversion near 1 km aligns with the sharp drop in aerosol concentration, suggesting limited vertical mixing. In Figure 7b, the height of the inversion increases, with the inversion occurring just below 2 km, consistent with the deeper mixed layer. Above these heights, aerosol concentrations remain small, with minor aerosol features aloft. As seen in Figure 7c, in the early evening (22:59–23:59 UTC), both BLH-RiB and BLH-LL dropped to around 0.9 km and coincide with a temperature inversion, consistent with early boundary-layer collapse. However, r_m remained elevated at around 2 km, suggesting a decoupling between the BLH and r_m as the boundary layer collapsed. At midnight (04:59–05:59 UTC; Figure

https://doi.org/10.5194/egusphere-2026-1748
Preprint. Discussion started: 2 April 2026

7d), the r_m remained around 1 km, while BLH-RiB (0.7 km) and BLH-LL (0.2 km) both fell below r_m. The sharpness of the transition zone is also weaker at midnight, with the lowest curve fitted k on this day (Table S.2). The diurnal aerosol vertical profile evolution shows that that aerosol vertical structure is coupled to the boundary layer during its growth but not its collapse. This phenomenon is typical for the nighttime boundary layer, when the residual layer remains aloft as a new nocturnal boundary layer forms (Bourgeois et al., 2018). This case study also shows that when the boundary layer collapses abruptly before sunset, rather than gradually weakening with reduced insolation, the aerosol layer can become decoupled from the surface before nighttime.

Elevated aerosol layers between 2 to 4 km can be seen in early evening (Figure 7c) and at midnight (Figure 7d). These layers coincide with a high-RH layer aloft and are bounded by upper-level inversions, consistent with stratification helping maintain vertical separation. However, this co-location does not establish causality or rule out a shared driver.

3.3 Case study: Sea breeze circulation and airmass impact on aerosol vertical distributions

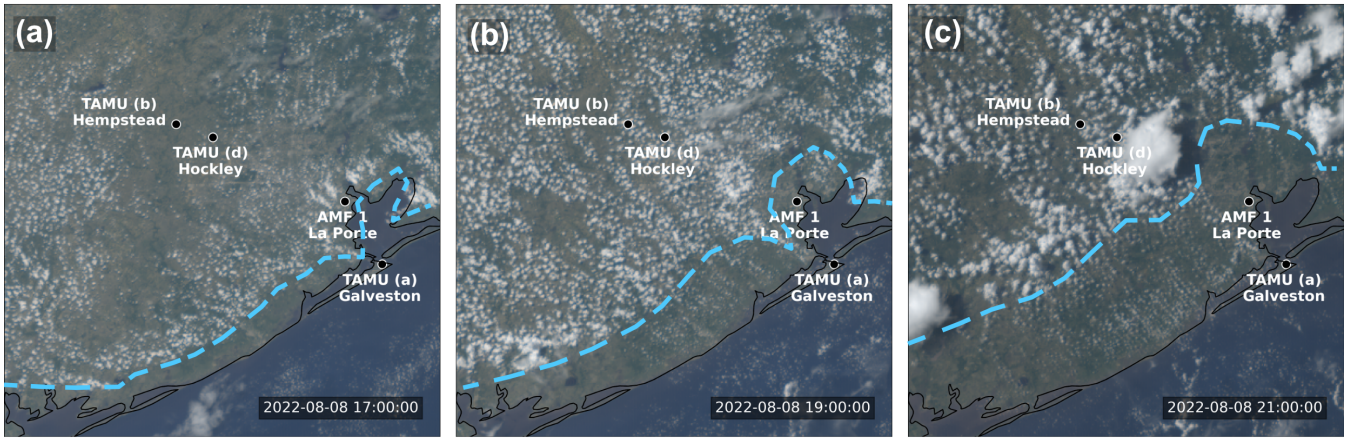

Figure 8 GOES16 Geocolor imagery on 8–9 August 2022, at 17:00 (a), 19:00 (b), and 21:00 UTC (c). The sea breeze front is marked in blue dashed lines. The campaign sites are labeled in white text.

The third case, on 8-9 August 2022, showcases the evolution of the aerosol vertical profile under the influence of a sea breeze circulation. On this day, the ROAM-V sampled at multiple TAMU sites: it began measurements in Galveston in the morning and later relocated inland to Hempstead, while AMF-1 operated continuously at La Porte. To visualize the progression of the sea-breeze front relative to the active ROAM-V location and AMF-1, Figure 8 presents GOES-16 Geocolor imagery (Miller et al., 2020). The sea breeze front was identified based on the characteristic inland advancing cumulus cloud bands visible in the satellite imagery (Planchon et al., 2006; Sharma et al., 2024). The sea breeze front marks a sharp boundary that separates cooler, moister maritime air along the coast from the continental air farther inland. According to Figure 8, by about 17:00 UTC, the sea breeze front had already passed the TAMU Galveston site but was only

https://doi.org/10.5194/egusphere-2026-1748
Preprint. Discussion started: 2 April 2026

just beginning to move across the AMF-1 site at La Porte. By 21:00 UTC, the sea breeze front had moved past the coastal sites at Galveston and La Porte but had not yet reached the inland TAMU Hempstead site.

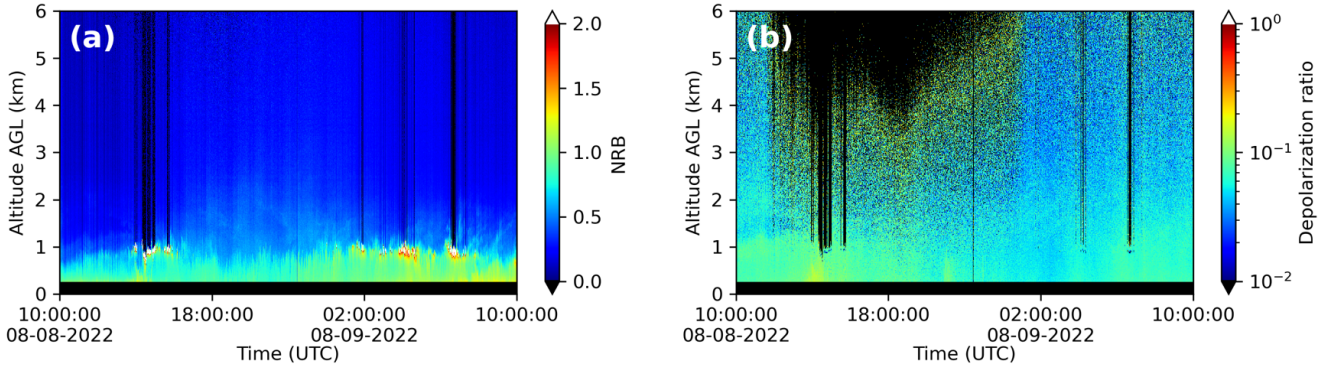

Figure 9 Micropulse lidar measurement from 10:00 UTC on 8 August to 10:00 UTC on 9 August 2022, at AMF-1 site (a) NRB time series (b) linear depolarization time series with signal to noise ratio > 3.

As seen in Figure 9, no notable elevated aerosol layers are observed on this day. The gradual change in 1–2 km backscatter around 16:00–02:00 UTC (18–19 May) may indicate some degree of vertical mixing. The depolarization ratio does not exhibit a distinct discontinuity in this layer, further suggesting that the transition is gradual rather than associated with a sharp inversion or elevated aerosol layer. This behavior is consistent with weak stratification and enhanced turbulent mixing.

https://doi.org/10.5194/egusphere-2026-1748
Preprint. Discussion started: 2 April 2026

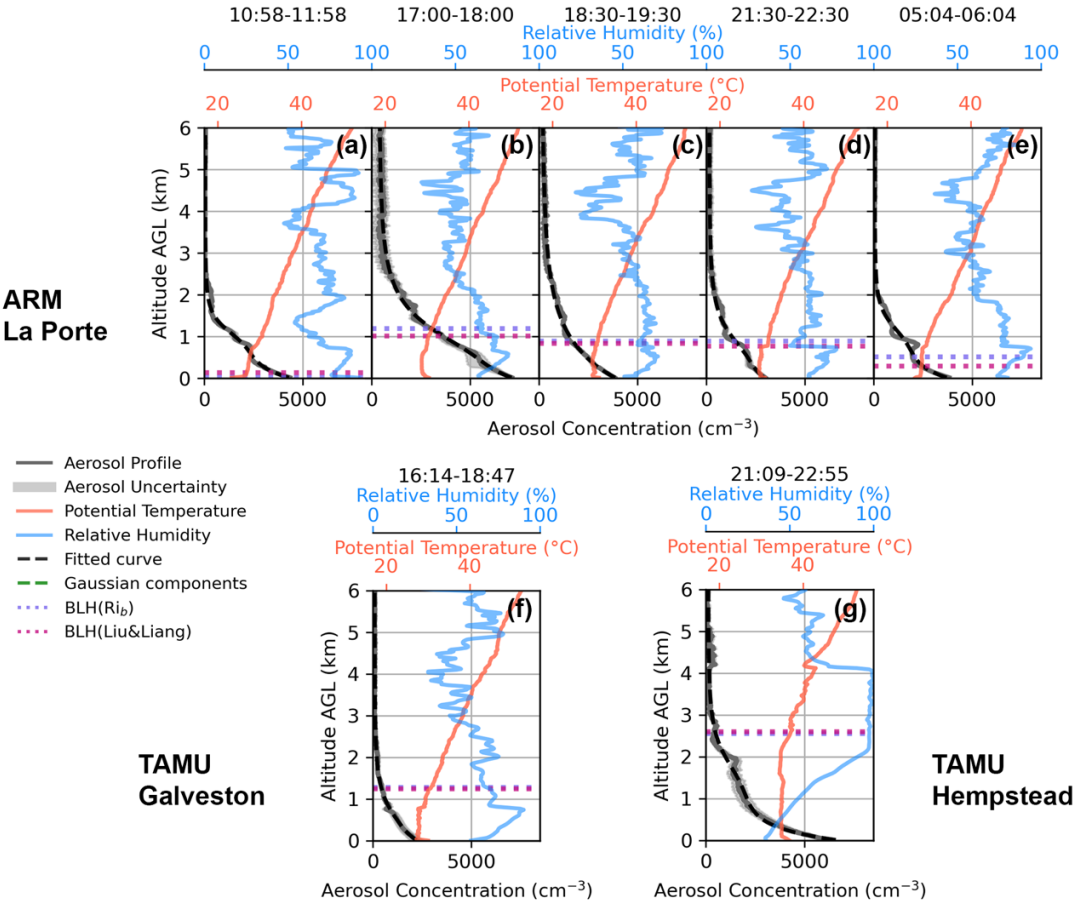

Figure 10 Measured vertical profiles of aerosol number concentration (gray solid lines), potential temperature profiles (solid red lines), relative humidity profile (solid blue lines), and curve fitted aerosol vertical profile (dashed black lines) at the AMF-1 site and two TAMU sites on 8–9 August 2022. Green dashed lines indicate Gaussian components added to represent elevated aerosol layers. Boundary layer heights determined by the bulk Richardson number and the Liu & Liang method are shown as purple and magenta dotted horizontal lines, respectively. The curve fit profile closely overlaps the measured number-concentration profiles, so the gray lines can be difficult to distinguish from the black dashed lines where agreement is good. Each panel corresponds to a one-hour averaging window in UTC time. AMF-1 site: (a) 10:58–11:58 on 8 August, (b) 17:00–18:00 on 8 August, (c) 18:30–19:30 on 8 August, (d) 21:30–22:30 on 8 August, and (e) 05:04–06:04 on 9 August. TAMU Galveston site (f) 16:14–18:47 on 8 August. TAMU Hempstead site (g) 21:09–22:55 on 8 August.

Aerosol concentration, potential temperature, and RH profiles, as well as BLHs at selected times at the AMF-1 site are shown in Figure 10. Corresponding profiles measured at the TAMU Galveston and Hempstead sites are also included (marked in Figure 10). For both ARM and TAMU Galveston sites, the potential temperature profiles have a distinctly different vertical structure compared to the previous two cases, featuring a much weaker inversion at around 0.8 km and less inhibition to vertical mixing. The aerosol profiles also appear less structured, with a smoother vertical gradient and no clear separation between layers as seen in the previous two cases. Since measurements from multiple sites are available on this day, we can investigate how the sea breeze circulation shapes aerosol vertical distributions across the urban coastal area.

https://doi.org/10.5194/egusphere-2026-1748
Preprint. Discussion started: 2 April 2026

This analysis compares the observed aerosol vertical profiles, the transition zone height r_m derived from Equation 1 curve fit, and the BLHs obtained from radiosonde measurements across the maritime and continental side of the sea breeze front.

At the AMF-1 site, the low-level aerosol concentration increases from 4400 cm^{-3} around early morning (10:58–11:58 UTC, Figure 10a), to 7200 cm^{-3} around noon (17:00–18:00 UTC, Figure 10b), likely due to the buildup of local emissions within a developing boundary layer. Shortly after, concentrations begin to decrease throughout the late afternoon and evening, reaching a minimum of around 2900 cm^{-3} in the late afternoon (21:30–22:30 UTC, Figure 10d). The decline in concentration coincides with the arrival of maritime air south of the sea breeze front, replacing the earlier continental air mass. Aerosol concentrations aloft follow a similar trend, with larger concentrations in the early afternoon that gradually decline into the evening. The fitted transition zone height r_m at the AMF-1 site is around 1.2 km throughout the day. Both BLH-RiB and BLH-LL agreed well, increasing from <0.2 km in late morning to about 1 km in early afternoon before gradually decreasing later in the day. The BLH remained shallow, peaking near 1 km after the sea breeze passage. The weak mixed-layer growth may explain the limited change in r_m. The sea breeze and the HYSPLIT back trajectories (Figure S.7 in the Supplement) indicate that the aerosol sampled at AMF1 were primarily of maritime origin.

At the TAMU Galveston site, from late morning to early afternoon (16:14–18:47 UTC), the aerosol vertical distributions resemble that observed at the AMF1 site in the afternoon (18:30–19:30 UTC), and the fitted transition zone height r_m at Galveston closely matches the r_m at the AMF1 site around noon (17:00–18:00 UTC) at around 1 km (see Table S.3 and S.4 in the Supplement). This similarity reflects the influx of maritime air behind the sea breeze front, which carries relatively cleaner marine air and establishes a boundary layer structure comparable at both locations once the sea breeze front has passed. HYSPLIT trajectories indicate Galveston air also arriving from the southeast over the Gulf, explaining its close resemblance to AMF-1 once the sea breeze has passed (Figure S.7 in the Supplement). At the TAMU Hempstead site in the late afternoon (21:09–22:55 UTC), aerosol concentrations throughout the profile were greater than at the coastal sites, and the fitted transition height r_m was about 1.94 km. The fitted r_m at the Hempstead site is also closer to the BLH, which is at around 2.5 km. The greater aerosol concentration and deeper transition region height are characteristic of the continental air mass that persists inland, rich in urban and biogenic emissions and less influenced by marine dilution. In addition, HYSPLIT trajectories for Hempstead remain near the surface until close to arrival of the sea breeze front (Fig. S.7 in the Supplement), supporting the interpretation that the site was influenced by a local or continental air mass, which helps explain the larger aerosol concentration and higher r_m observed there.

The comparison between the aerosol vertical distributions at different sites and times of the day reveals that the aerosol vertical distributions can have strong spatial heterogeneity, especially when there is a sea breeze circulation. During TRACER, near-surface aerosol properties differed systematically between polluted-marine and continental airmasses

https://doi.org/10.5194/egusphere-2026-1748
Preprint. Discussion started: 2 April 2026

(Thompson et al., 2025a). This case study shows that, in a coastal urban environment like the Greater Houston area, the aerosol vertical distributions can be affected by sea breeze circulation and air mass transitions.

3.4 Relationship between Boundary Layer Height and Aerosol Vertical Profile

The AMF-1 deployment in the Greater Houston area offers a large dataset to study which environmental predictors are associated with and can potentially be used to predict the shape of aerosol vertical profiles. Six months of data from March 2022 to September 2022 were curve fitted using Equation 1 or Equation 2. Because automated elevated-aerosol layer detection was not implemented for this study, Equation 1 was first used to fit all profiles. The profiles fit with $R^2 < 0.98$ and visually classified as containing an elevated aerosol layer were then refit using Equation 2 with one or two gaussian terms. A profile was classified as having an elevated layer when it showed a distinct local maximum in aerosol concentration above the low-level aerosol layer and was separated from it by a relative local minimum. After model selection, only profiles with final fit quality $R^2 > 0.98$ were retained for the statistical analysis to ensure that the fitted parameters represented well-resolved profile structure. Overall, 144 of 313 profiles met this strict quality criterion. The frequency distributions of fitted parameters are presented in the supporting information in Figure S.8. As shown qualitatively in the case studies, we observe that BLH and r_m may have a positive correlation during the daytime. Comparing the case studies, a more abrupt transition from the low-level aerosol-rich layer to the air aloft, quantified by a larger k, is associated with stronger potential-temperature inversions. As we observed, the aerosol profiles on 18–19 May 2022 exhibit both a tighter transition zone and a steeper transition (larger k) than the profiles on 8–9 August 2022. Motivated by these patterns, we compare BLH and stability with the curve-fitted transition height r_m and the shape parameter k. For reference, we also provide the corresponding BLH–r_m and stability–k scatter plots obtained when Equation 1 is applied to all profiles (i.e., without elevated-layer refitting) in the Supplement (Figures S9–S10).

https://doi.org/10.5194/egusphere-2026-1748
Preprint. Discussion started: 2 April 2026

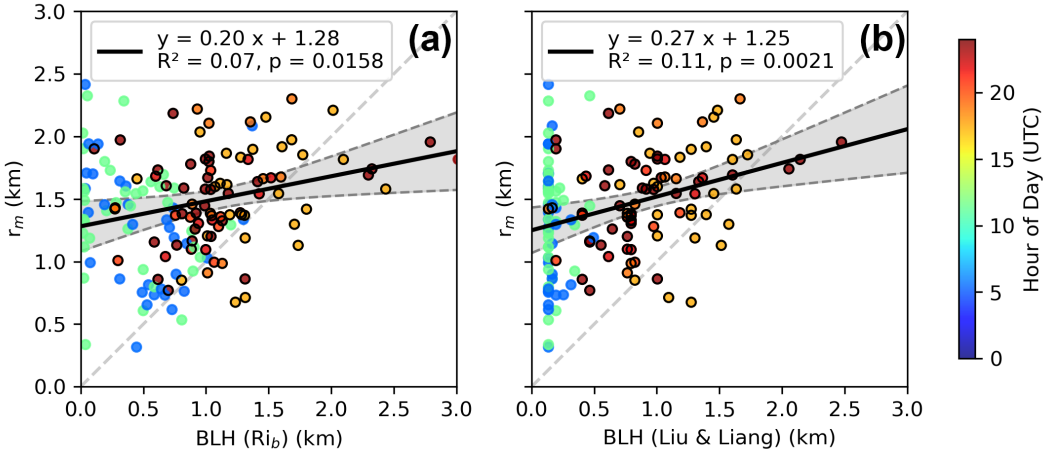

Figure 11 Sensitivity of boundary layer height–r_m comparison to fitting formulation (a) Comparison between boundary layer heights derived from the bulk Richardson number method and the curve fitted r_m (b) Comparison between BLHs obtained with the Liu & Liang (2010) thermodynamic method and the r_m. The scattered points are color coded by the hour of day (UTC), with warmer colors corresponding to daytime hours. Points corresponding to daytime hours (12:00–23:00 UTC) are additionally highlighted with black outlines. The linear regression line is shown in a solid black line and is only performed on daytime datapoints. The 95 % confidence interval is shown as a darker gray band bounded by dashed lines. The 95 % prediction interval is added as a lighter gray band bounded by dotted lines.

In Figure 11, we compare the thermodynamically determined BLH from radiosonde data with the curve fitted transition zone height r_m to examine how the BLH covaries with structure of the aerosol vertical profiles using available data from March and September 2022 measured at the AMF-1 site. Comparison between the curve fitted transition height r_m and BLH shows that r_m tends to be systematically higher, as most data points lie above the 1:1 reference line. This overestimation may reflect the fact that aerosol layers often extend above the diagnosed boundary layer, particularly when the boundary layer is not well mixed. As shown in Figure 11, BLH values are greater during the daytime and can reduce the discrepancy between r_m and BLH. In contrast, during nighttime or under stable stratification conditions, the diagnosed BLH becomes much shallower, while elevated aerosol layers may persist. In these cases, the Liu and Liang (2010) method appears more effective at capturing shallow stable boundary layers than the Richardson number method, potentially providing a closer match to the aerosol-defined transition height during daytime.

We performed linear regression analysis using daytime data only, comparing the fitted aerosol transition height r_m with BLH derived from both the Richardson number and Liu & Liang methods. We find a weak but statistically significant positive correlation between the curve fitted transition height r_m and the BLH. The relationship is stronger when using the BLH-LL ($R^2 = 0.11$, $p = 0.0021$) than when using the BLH-RiB ($R^2 = 0.07$, $p = 0.0158$). The positive correlation indicates that higher BLHs are generally associated with deeper aerosol transition heights, suggesting that BLH plays a contributing role in shaping the aerosol vertical structure. However, the relatively low R^2 shows that the BLH only explains a small fraction of the variability in r_m.

https://doi.org/10.5194/egusphere-2026-1748
Preprint. Discussion started: 2 April 2026

435 The limited explanatory power of BLH likely reflects several contributing factors. First, the aerosol vertical profile is shaped not only by the instantaneous thermodynamic structure, but also by the boundary layer's recent evolution. As seen in the case study of 21 July 2022, during boundary layer growth, surface emitted aerosols become mixed throughout a deepening layer. As BLH decays, previously mixed aerosols can remain aloft even as the boundary layer becomes shallow, causing a mismatch between BLH and r_m. Second, aerosol layers from long range transport can reside over the local boundary layer
440 and later subside and merge with near surface aerosol layer. Even with additional Gaussian peaks, the fitting routine may not always cleanly separate the transported signal from locally emitted aerosols. And finally, uncertainties in both BLH diagnostics and the aerosol curve fitting, particularly under weak stratification or merged layers, can mask the link between BLH and r_m.

445 In conclusion, although BLH exhibits a weak but statistically significant positive correlation with the fitted transition height r_m, BLH explains only a small fraction of the variability in r_m. This result indicates that BLH alone cannot reliably determine the depth of the near-surface aerosol layer or the overall structure of the aerosol vertical profile.

3.5 Relationship between Thermodynamic Stability and Aerosol Vertical Profile

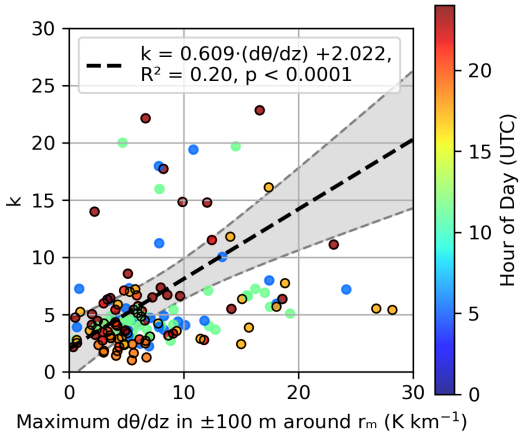

450 **Figure 12 Sensitivity of stability–k relationship to fitting formulation. Comparison between local maximum potential temperature gradient (dθ/dz, evaluated within ±100 m around curve fitted r_m) and curve fitted k results based on AMF-1 data. Points corresponding to daytime hours (12:00–23:00 UTC) are additionally highlighted with black outlines. The linear regression line is shown in a solid black line. The 95 % confidence interval is shown as a darker gray band bounded by dashed lines. The 95 % prediction interval is added as a lighter gray band bounded by dotted lines.**

455 We then examine whether the local vertical gradient in potential temperature (i.e., the static stability) can help explain variations in k. Since atmospheric stability influences vertical mixing and stratification, a stronger gradient in potential

https://doi.org/10.5194/egusphere-2026-1748
Preprint. Discussion started: 2 April 2026

temperature is expected to be associated with a steeper vertical aerosol gradient, k, at the transition zone, r_m. The local maximum vertical gradient of potential temperature (dθ/dz) was calculated within ±100 m of the fitted transition height r_m, using smoothed radiosonde profiles to reduce high frequency noise. The smoothing was performed with a Gaussian kernel with a full width at half maximum of 100 m, consistent with common boundary layer profiling practice of applying vertical averaging at a scale of tens of meters (Bhimireddy and Kristovich, 2024). The comparison between static stability and k is shown as a scatterplot in Figure 12.

A statistically significant ($p << 0.01$) and limited positive correlation ($R^2 = 0.20$) is found between the potential temperature gradient at r_m and the curve-fitted transition sharpness parameter k. This result shows that the local atmospheric stability near r_m appears to play a critical role in shaping the vertical profile, as stronger stability suppresses vertical mixing and leads to a sharper transition in aerosol concentration. In contrast, weaker stability may allow for more gradual mixing across layers, resulting in a more diffuse transition zone and smaller k values. These findings show that the potential temperature gradient near r_m may therefore serve as a physically grounded parameter for representing the strength of aerosol stratification in modeling frameworks.

https://doi.org/10.5194/egusphere-2026-1748
Preprint. Discussion started: 2 April 2026

3.6 Demonstration of Aerosol Vertical Profile Prediction

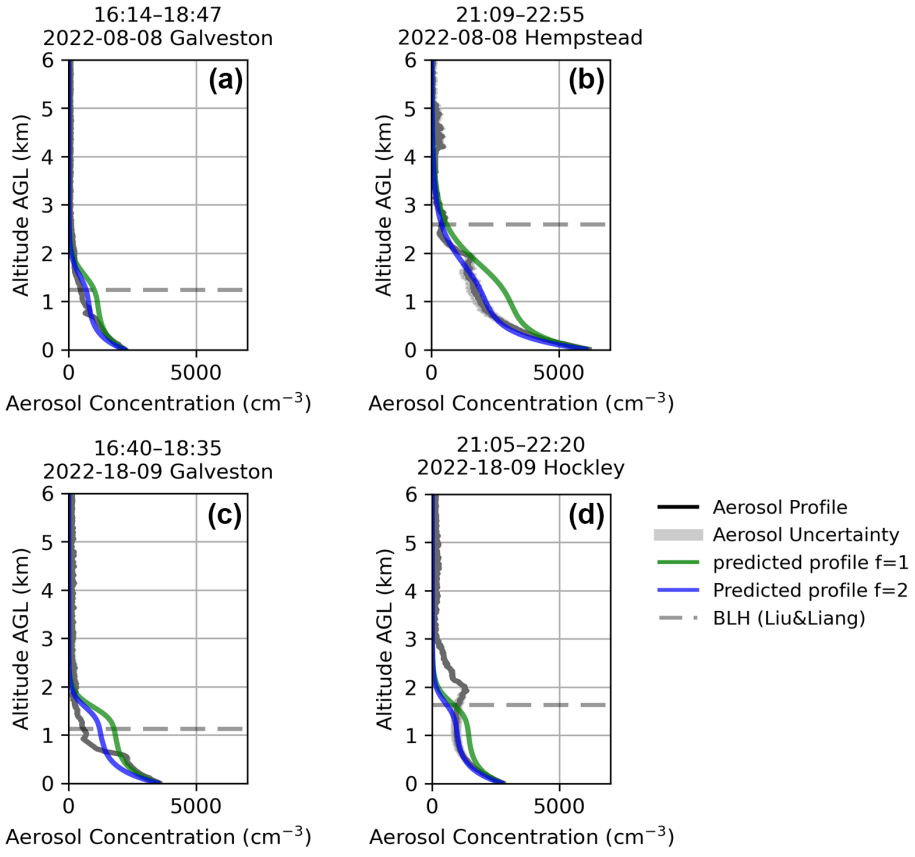

Figure 13 Demonstration of aerosol vertical profile prediction with TAMU data using the curve fitting equation and parameterization derived from AMF-1 site observations. (a) 16:14–18:47 UTC on 8 August 2022 at Galveston site, (b) 21:09–22:55 UTC on 8 August 2022 at Hempstead site (c) 16:40–18:35 UTC on 18 September 2022 at Galveston site (d) 21:05–22:20 UTC on 18 September 2022 at Hockley site. The aerosol profile is shown in black. The predicted profiles using f = 1 are shown as the green line, and the predicted profiles using f = 2 are shown as the blue line. The BLH-LL is marked with a horizontal gray dashed line.

Building on the established, albeit weak, relationships between BLH and local potential temperature gradients on aerosol vertical profiles, we next examine whether these variables can be used to predict the shape of the aerosol vertical profile without vertical lidar measurements. Given its stronger correlation with the transition height r_m, the Liu and Liang (2010) based BLH is used in the following analysis. The transition height r_m is estimated using the linear regression relationship with the Liu and Liang (2010) based BLH, expressed as $r_m = 0.27 \times BLH + 1.25$ km. The sharpness of the transition zone k is then estimated as $k = 0.609 \times (\frac{d\theta}{dz})_{max, r_m \pm 100\text{m}} + 2.022$. γ is set as 0.3, consistent with the previous curve fitting. Since a predictive relationship was not found for f, fixed values of $f = 1$ and $f = 2$ are selected for testing, guided by the distribution shown in Figure S.8, where the mode of f is centered around 1.1. The aerosol concentration measured on the surface is used for X_0, and a concentration of 10 cm^{-3} is chosen for X_f. The prediction equation then becomes:

https://doi.org/10.5194/egusphere-2026-1748
Preprint. Discussion started: 2 April 2026

$$X(r) = \frac{X_0 - 10}{1+f} \cdot \frac{1 + f e^{-\frac{r}{0.3}}}{1 + \left(\frac{r}{0.27 \times BLH + 1.25}\right)^{(0.27 \times BLH + 1.25)\left(k = 0.609 \times \left(\frac{d\theta}{dz}\right)_{max,\, r_m \pm 100\mathrm{m}} + 2.022\right)}} + 10 \quad (3)$$

The TAMU coastal and inland site's aerosol vertical profiles for 8 August and 18 September were chosen for the demonstration. The TAMU site was not included in the derivation of the empirical relationships from the ARM dataset, allowing for an independent evaluation of how well the thermodynamic structure predicts aerosol profile structure at a different location. Although the predictive relationships for r_m and k are only weak to moderate, it is nonetheless valuable to explore how well these variables, derived from thermodynamic structure, can approximate aerosol profiles, particularly in situations where direct vertical measurements are unavailable and estimates are required.

As seen in Figure 13, the prediction worked well for 8 August for both sites using $f = 2$, with a higher R^2 at 0.96 compared to the prediction using $f = 1$ with a R^2 at 0.89. However, for the 18 September cases, the transition height r_m is not accurately predicted based on BLH. In the noon (16:40–18:35 UTC) profile (Figure 13c), the predicted r_m is too high, while in the late afternoon (21:05–22:20 UTC) profile (Figure 13d) it is too low. These discrepancies highlight the limitations of using BLH alone to predict the height of aerosol transition zone, as the BLH is not a strong predictor of r_m as we previously demonstrated. These results show that accurate prediction of the vertical aerosol profile depends on the reliable estimation of the transition zone height r_m. An improved prediction of r_m would also improve the estimation of the sharpness parameter k. Additionally, the factor f has a strong influence on the shape of the aerosol profile and thus requires further investigation.

4. Conclusion

In this work, we investigated how the vertical distributions of aerosols are related to boundary layer characteristics in a coastal urban environment, using data collected during the 2022 TRACER campaign in Greater Houston, Texas. We first developed an empirical model to describe aerosol vertical profiles from lidar observations, then compared the fitted profiles with thermodynamic profiles to assess how boundary layer processes affect aerosol vertical profiles. We examined case studies to illustrate how processes such as convective growth, the nocturnal stable boundary layer, and sea breeze circulation influence aerosol vertical structure. We also analyzed six months of data to evaluate the statistical relationships of aerosol profile features with BLH and static stability and demonstrated a preliminary framework for predicting aerosol profiles based on these variables.

In addressing our research goals, we find that the typical aerosol vertical profile in the Greater Houston coastal urban environment is S-shaped, with largest concentrations near the surface, relatively constant concentrations in the lowest 1-2 km above the surface layer associated with vertical mixing in the boundary layer, and a sharp decrease in a "transition zone",

https://doi.org/10.5194/egusphere-2026-1748
Preprint. Discussion started: 2 April 2026

which is often (but not always) at or above the boundary layer capping inversion; at nighttime, a residual layer of aerosol remains aloft, above the stable nocturnal boundary layer. This S-shape becomes more pronounced under stronger inversions or more stable boundary layer conditions, which suppress vertical mixing and sharpen the aerosol transition zone. Boundary layer processes, including convective atmospheric boundary-layer development, collapse, and sea breeze-driven circulation influence the shape of the aerosol profile, as demonstrated in our case studies and six-month analysis. We demonstrate that aerosol vertical profiles are only weakly related to BLH and thermodynamic stability. Though much of the variance is unexplained by these variables, they may still offer a practical framework for predicting aerosol vertical profile when airborne or lidar measurement are not available. These findings highlight the relationship between boundary layer properties and aerosol vertical distributions and establish a physically grounded basis for future profile prediction. The aerosol vertical profile fitting function developed in this study can also be applied to parameterize aerosol vertical profiles in numerical weather or climate models or provide constraints for remote sensing retrieval algorithms.

Our findings corroborate previous observations linking the aerosol vertical profile to boundary-layer structure (Sun et al., 2024; Li et al., 2022; Ware et al., 2016; Thomas et al., 2019; Prasad et al., 2022). However, most lidar studies have used optical profiles like the extinction coefficient profile, which are strongly influenced by hygroscopic growth in humid air. Because moisture is also controlled by boundary-layer processes, extinction-based metrics can overestimate the link to those processes by reflecting particle growth rather than actual concentration changes. We instead apply a correction for hygroscopic growth to backscatter profiles, reducing humidity-related biases and providing a clearer view of how the boundary layer processes shape aerosol vertical distributions.

One caveat is that these fitted relationships and parameter values are derived from a limited set of cases in the Houston coastal–inland regime during TRACER, and their applicability to other seasons, locations, and boundary-layer regimes remains uncertain. A logical next step is to apply the same curve-fitting framework at other ARM sites and evaluate how the fitted parameters relate to meteorological conditions across a broader range of regimes. Also, incorporating the evolution of the boundary layer over the preceding several hours into aerosol vertical-profile predictions, rather than relying solely on conditions at the time of measurement, may improve predictive skill. This is motivated by our finding that the BLH at the time of measurement is a weak predictor of aerosol vertical structure. Another improvement would be to incorporate long-term in situ sampling, for example, using tethered balloons or small drones to capture the behavior of ultrafine aerosols in the nucleation and accumulation modes, which are not detectable by an elastic lidar. In addition, the decay parameters γ and f, which control how sharply concentration decreases with height below r_m, remain loosely constrained and likely reflect the combined effects of turbulent mixing, entrainment at the boundary-layer top, surface emissions, gravitational settling, and boundary layer stability.

https://doi.org/10.5194/egusphere-2026-1748
Preprint. Discussion started: 2 April 2026

5 Data Availability

The data used in this analysis are publicly available from the DOE Atmospheric Radiation Measurement (ARM) Data Archive: https://armgov.svcs.arm.gov/research/campaigns/osc2022tracer-tamu/ (last access: 31 March 2026; https://doi.org/10.5439/1972461, https://doi.org/10.5439/1968819, https://doi.org/10.5439/1972179) and https://armgov.svcs.arm.gov/research/campaigns/amf2021tracer/ (last access: 31 March 2026; https://doi.org/10.5439/1320657, https://doi.org/10.5439/1871375, https://doi.org/10.5439/1595321, https://doi.org/10.5439/1763029). Additional data are available from Texas data repository: https://doi.org/10.18738/T8/NUX5AZ (last access: 31 March 2026).

6 Code Availability

The code used in this study is currently available from the corresponding author upon request.

7 Author Contribution

S.D.B. conceived of the project. B.C. and S.D.B. designed the analysis and led the writing of the manuscript. B.C., S.A.T., B.H.M., M.S., C.J.N., A.D.R., and R.L. collected and curated the data. M.S. C.J.N. and A.D.R. contributed to the data interpretation and writing of the manuscript.

8 Competing Interest

The authors declare that they have no conflict of interest.

9 Acknowledgement

This research was funded by the U.S. Department of Energy's Atmospheric System Research (DOE ASR) Program under award #DE-SC0021047 and #DE-SC0025215.

https://doi.org/10.5194/egusphere-2026-1748
Preprint. Discussion started: 2 April 2026

References

Albrecht, B. A.: Aerosols, cloud microphysics, and fractional cloudiness, Science, 245, 1227–1230, https://doi.org/10.1126/science.245.4923.1227, 1989.

Bhimireddy, S. R. and Kristovich, D. A.: Identification of convective boundary layer depth over the great lakes region using aircraft observations: A comparison of various methods, Journal of Applied Meteorology and Climatology, 63, 401–423, 2024.

Bourgeois, Q., Ekman, A. M., Renard, J.-B., Krejci, R., Devasthale, A., Bender, F. A.-M., Riipinen, I., Berthet, G., and Tackett, J. L.: How much of the global aerosol optical depth is found in the boundary layer and free troposphere?, Atmospheric Chemistry and Physics, 18, 7709–7720, https://doi.org/10.5194/acp-18-7709-2018, 2018.

Burrows, S. M., McCluskey, C. S., Cornwell, G., Steinke, I., Zhang, K., Zhao, B., Zawadowicz, M., Raman, A., Kulkarni, G., and China, S.: Ice-nucleating particles that impact clouds and climate: Observational and modeling research needs, Reviews of Geophysics, 60, e2021RG000745, 2022.

Chen, B., Thompson, S. A., Matthews, B. H., Sharma, M., Li, R., Nowotarski, C. J., Rapp, A. D., and Brooks, S. D.: A new technique to retrieve aerosol vertical profiles using micropulse lidar and ground-based aerosol measurements, Atmospheric Measurement Techniques, 18, 5841–5859, https://doi.org/10.5194/amt-18-5841-2025, 2025.

Choi, J.-O. and Chung, C. E.: Sensitivity of aerosol direct radiative forcing to aerosol vertical profile, Tellus B: Chemical and Physical Meteorology, 66, 24376, https://doi.org/10.3402/tellusb.v66.24376, 2014.

Clarke, A. and Kapustin, V.: Hemispheric aerosol vertical profiles: Anthropogenic impacts on optical depth and cloud nuclei, Science, 329, 1488–1492, https://doi.org/10.1126/science.1188838, 2010.

Fan, J., Wang, Y., Rosenfeld, D., and Liu, X.: Review of aerosol–cloud interactions: Mechanisms, significance, and challenges, Journal of the Atmospheric Sciences, 73, 4221–4252, https://doi.org/10.1175/JAS-D-16-0037.1, 2016.

Freire, L., Chamecki, M., and Gillies, J.: Flux-profile relationship for dust concentration in the stratified atmospheric surface layer, Boundary-layer meteorology, 160, 249–267, https://doi.org/10.1007/s10546-016-0140-2, 2016.

Haman, C. L., Lefer, B., and Morris, G. A.: Seasonal variability in the diurnal evolution of the boundary layer in a near-coastal urban environment, Journal of Atmospheric and Oceanic Technology, 29, 697–710, 2012.

Haywood, J. and Boucher, O.: Estimates of the direct and indirect radiative forcing due to tropospheric aerosols: A review, Reviews of geophysics, 38, 513–543, https://doi.org/10.1029/1999RG000078, 2000.

Hoppel, W., Frick, G., and Fitzgerald, J.: Surface source function for sea-salt aerosol and aerosol dry deposition to the ocean surface, Journal of Geophysical Research: Atmospheres, 107, AAC 7–1–AAC 7–17, https://doi.org/10.1029/2001JD002014, 2002.

Jensen, M. P., Flynn, J. H., Gonzalez-Cruz, J. E., Judd, L. M., Kollias, P., Kuang, C., McFarquhar, G. M., Powers, H., Ramamurthy, P., and Sullivan, J.: Studying Aerosol, Clouds, and Air Quality in the Coastal Urban Environment of Southeastern Texas, Bulletin of the American Meteorological Society, BAMS–D–23–0331.0331, https://doi.org/10.1175/BAMS-D-23-0331.1, 2025.

Johnson, B., Shine, K., and Forster, P.: The semi-direct aerosol effect: Impact of absorbing aerosols on marine stratocumulus, Quarterly Journal of the Royal Meteorological Society, 130, 1407–1422, https://doi.org/10.1256/qj.03.61, 2004.

Kahn, R. A.: Reducing the uncertainties in direct aerosol radiative forcing, Surveys in geophysics, 33, 701–721, https://doi.org/10.1007/s10712-011-9153-z, 2012.

Kanji, Z. A., Ladino, L. A., Wex, H., Boose, Y., Burkert-Kohn, M., Cziczo, D. J., and Krämer, M.: Overview of ice nucleating particles, Meteorological monographs, 58, 1.1–1.33, 2017.

Kipling, Z., Stier, P., Johnson, C. E., Mann, G. W., Bellouin, N., Bauer, S. E., Bergman, T., Chin, M., Diehl, T., and Ghan, S. J.: What controls the vertical distribution of aerosol? Relationships between process sensitivity in HadGEM3–UKCA and inter-model variation from AeroCom Phase II, Atmospheric Chemistry and Physics, 16, 2221–2241, https://doi.org/10.5194/acp-16-2221-2016, 2016.

Lamer, K., Mages, Z., Treserras, B. P., Walter, P., Zhu, Z., Rapp, A. D., Nowotarski, C. J., Brooks, S. D., Flynn, J., and Sharma, M.: Spatially distributed atmospheric boundary layer properties in Houston–A value-added observational dataset, Scientific Data, 11, 661, https://doi.org/10.1038/s41597-024-03477-9, 2024.

Lebo, Z. J.: The sensitivity of a numerically simulated idealized squall line to the vertical distribution of aerosols, Journal of the Atmospheric Sciences, 71, 4581–4596, https://doi.org/10.1175/JAS-D-14-0068.1, 2014.

https://doi.org/10.5194/egusphere-2026-1748
Preprint. Discussion started: 2 April 2026

Lei, Z., Peña, T., Thompson, S. A., Chen, B., Matthews, B. H., Li, R., Rapp, A. D., Nowotarski, C. J., and Brooks, S. D.: Aerosol Physicochemical Mixing State and Cloud Nucleation Potential during Tracking Aerosol Convection Interactions Experiment (TRACER) Campaign, Environmental Science & Technology, https://doi.org/10.1021/acs.est.5c03508, 2025.

Li, H., Liu, B., Ma, X., Ma, Y., Jin, S., Fan, R., Wang, W., Fang, J., Zhao, Y., and Gong, W.: The influence of temperature inversion on the vertical distribution of aerosols, Remote Sensing, 14, 4428, https://doi.org/10.3390/rs14184428, 2022.

Lin, Y., Takano, Y., Gu, Y., Wang, Y., Zhou, S., Zhang, T., Zhu, K., Wang, J., Zhao, B., and Chen, G.: Characterization of the aerosol vertical distributions and their impacts on warm clouds based on multi-year ARM observations, Science of The Total Environment, 904, 166582, https://doi.org/10.1016/j.scitotenv.2023.166582, 2023.

Liu, S. and Liang, X.-Z.: Observed diurnal cycle climatology of planetary boundary layer height, Journal of Climate, 23, 5790–5809, https://doi.org/10.1175/2010JCLI3552.1, 2010.

Marinescu, P. J., van den Heever, S. C., Saleeby, S. M., Kreidenweis, S. M., and DeMott, P. J.: The microphysical roles of lower-tropospheric versus midtropospheric aerosol particles in mature-stage MCS precipitation, Journal of the Atmospheric Sciences, 74, 3657–3678, https://doi.org/10.1175/JAS-D-16-0361.1, 2017.

Miller, S. D., Lindsey, D. T., Seaman, C. J., and Solbrig, J. E.: GeoColor: A blending technique for satellite imagery, Journal of Atmospheric and Oceanic Technology, 37, 429–448, https://doi.org/10.1175/JTECH-D-19-0134.1, 2020.

Mishra, A. K., Koren, I., and Rudich, Y.: Effect of aerosol vertical distribution on aerosol-radiation interaction: A theoretical prospect, Heliyon, 1, https://doi.org/10.1016/j.heliyon.2015.e00036, 2015.

Nissanka, I. D., Park, H. J., Freire, L. S., Chamecki, M., Reid, J. S., and Richter, D. H.: Parameterized vertical concentration profiles for aerosols in the marine atmospheric boundary layer, Journal of Geophysical Research: Atmospheres, 123, 9688–9702, https://doi.org/10.1029/2018JD028820, 2018.

Planchon, O., Damato, F., Dubreuil, V., and Gouéry, P.: A method of identifying and locating sea-breeze fronts in north-eastern Brazil by remote sensing, Meteorological Applications, 13, 225–234, https://doi.org/10.1017/S1350482706002283, 2006.

Prasad, P., Basha, G., and Ratnam, M. V.: Is the atmospheric boundary layer altitude or the strong thermal inversions that control the vertical extent of aerosols?, Science of The Total Environment, 802, 149758, https://doi.org/10.1016/j.scitotenv.2021.149758, 2022.

Rapp, A. D., Brooks, S. D., Nowotarski, C. J., Sharma, M., Thompson, S. A., Chen, B., Matthews, B. H., Etten-Bohm, M., Nielsen, E. R., and Li, R.: TAMU TRACER: Targeted Mobile Measurements to Isolate the Impacts of Aerosols and Meteorology on Deep Convection, Bulletin of the American Meteorological Society, https://doi.org/10.1175/BAMS-D-23-0218.1, 2024.

Seinfeld, J. H., Bretherton, C., Carslaw, K. S., Coe, H., DeMott, P. J., Dunlea, E. J., Feingold, G., Ghan, S., Guenther, A. B., and Kahn, R.: Improving our fundamental understanding of the role of aerosol−cloud interactions in the climate system, Proceedings of the National Academy of Sciences, 113, 5781–5790, https://doi.org/10.1073/pnas.1514043113, 2016.

Sharma, M., Rapp, A. D., Nowotarski, C. J., and Brooks, S. D.: Observed Variability in Convective Cell Characteristics and Near-Storm Environments across the Sea-and Bay-Breeze Fronts in Southeast Texas, Monthly Weather Review, 152, 2419–2441, https://doi.org/10.1175/MWR-D-23-0243.1, 2024.

Stull, R. B.: An introduction to boundary layer meteorology, Springer Science & Business Media, https://doi.org/10.1007/978-94-009-3027-8, 2012.

Sun, X., Zhou, Y., Zhao, T., Fu, W., Wang, Z., Shi, C., Zhang, H., Zhang, Y., Yang, Q., and Shu, Z.: Vertical distribution of aerosols and association with atmospheric boundary layer structures during regional aerosol transport over central China, Environmental Pollution, 362, 124967, https://doi.org/10.1016/j.envpol.2024.124967, 2024.

Szopa, S., Naik, V., Adhikary, B., Artaxo, P., Berntsen, T., Collins, W. D., Fuzzi, S., Gallardo, L., Kiendler-Scharr, A., and Klimont, Z.: Short-Lived Climate Forcers (Chapter 6), IPCC 2021: Climate Change 2021: The Physical Science Basis. Contribution of Working Group I to the Sixth Assessment Report of the Intergovernmental Panel on Climate Change, 817–922, 10.1017/9781009157896, 2023.

Thomas, M. A., Devasthale, A., Tjernström, M., and Ekman, A. M.: The relation between aerosol vertical distribution and temperature inversions in the Arctic in winter and spring, Geophysical Research Letters, 46, 2836–2845, https://doi.org/10.1029/2018GL081624, 2019.

https://doi.org/10.5194/egusphere-2026-1748
Preprint. Discussion started: 2 April 2026

Thompson, S. A., Chen, B., Matthews, B. H., Li, R., Nowotarski, C. J., Rapp, A. D., and Brooks, S. D.: Characterizing Greater Houston's aerosol by air mass during TRACER, Journal of Geophysical Research: Atmospheres, 130, e2025JD043353D, https://doi.org/10.1029/2025JD043353, 2025a.

Thompson, S. A., Peña, T. A., Chen, B., Sharma, M., Matthews, B. H., Li, R., Nowotarski, C. J., Rapp, A. D., and Brooks, S. D.: Variability in ice nucleating particles across Greater Houston Texas, Journal of Geophysical Research: Atmospheres, 130, e2025JD044164, https://doi.org/10.1029/2025JD044164, 2025b.

Twomey, S.: The influence of pollution on the shortwave albedo of clouds, Journal of the atmospheric sciences, 34, 1149–1152, https://doi.org/10.1175/1520-0469(1977)034%3C1149:TIOPOT%3E2.0.CO;2, 1977.

Ware, J., Kort, E. A., DeCola, P., and Duren, R.: Aerosol lidar observations of atmospheric mixing in Los Angeles: Climatology and implications for greenhouse gas observations, Journal of Geophysical Research: Atmospheres, 121, 9862–9878, https://doi.org/10.1002/2016JD024953, 2016.

Watson-Parris, D., Schutgens, N., Reddington, C., Pringle, K. J., Liu, D., Allan, J. D., Coe, H., Carslaw, K. S., and Stier, P.: In situ constraints on the vertical distribution of global aerosol, Atmospheric Chemistry and Physics, 19, 11765–11790, https://doi.org/10.5194/acp-19-11765-2019, 2019.

Xiao, J. and Taylor, P. A.: On equilibrium profiles of suspended particles, Boundary-Layer Meteorology, 105, 471–482, https://doi.org/10.1023/A:1020395323626, 2002.

Zhang, M., Deng, X., Zhu, R., Ren, Y., and Xue, H.: The impact of aerosol vertical distribution on a deep convective cloud, Atmosphere, 12, 675, https://doi.org/10.3390/atmos12060675, 2021.

Zhang, Q., Ma, X., Tie, X., Huang, M., and Zhao, C.: Vertical distributions of aerosols under different weather conditions: Analysis of in-situ aircraft measurements in Beijing, China, Atmospheric Environment, 43, 5526–5535, https://doi.org/10.1016/j.atmosenv.2009.05.037, 2009.

Zhang, X., Zheng, Y., Che, H., Gui, K., Li, L., Zhao, H., Liang, Y., Yao, W., Zhang, X., and Zhao, H.: Seasonal and diurnal characteristics of the vertical profile of aerosol optical properties in urban Beijing, 2017–2021, Remote Sensing, 15, 475, https://doi.org/10.3390/rs15020475, 2023.